

Direct and sequential radiative three-body reaction rates at low temperatures

E. Garrido¹, R. de Diego¹, D.V. Fedorov² and A.S. Jensen²

¹ Instituto de Estructura de la Materia, CSIC, Serrano 123, E-28006 Madrid, Spain

² Department of Physics and Astronomy, Aarhus University, DK-8000 Aarhus C, Denmark

Received: date / Revised version: date

Abstract. We investigate the low-temperature reaction rates for radiative capture processes of three particles. We compare direct and sequential capture mechanisms and rates using realistic phenomenological parametrizations of the corresponding photodissociation cross sections. Energy conservation prohibits sequential capture for energies smaller than that of the intermediate two-body structure. A finite width or a finite temperature allows this capture mechanism. We study generic effects of positions and widths of two- and three-body resonances for very low temperatures. We focus on nuclear reactions relevant for astrophysics, and we illustrate with realistic estimates for the α - α - α and α - α - n radiative capture processes. The direct capture mechanism leads to reaction rates which for temperatures smaller than 0.1 GK can be several orders of magnitude larger than those of the NACRE compilation.

PACS. 21.45.-v Few-body systems – 25.40.Lw Radiative capture – 26.20.-f Hydrostatic stellar nucleosynthesis

1 Introduction

The techniques employed to solve few-body problems have improved substantially over the last decade. This is not only due to the computer development but also to the higher efficiency of both the theoretical formulations and the numerical methods. In particular, a number of three-body problems are now all solvable at least within a certain requirement for the accuracy. The easiest of these problems are bound states [1,2] and perhaps resonances [3,4,5,6,7,8], whereas the more challenging are continuum structures in general [9,10,11]. The most demanding are reactions where the structures before and after the process are different [12,13,14].

Applications to nuclear astrophysics have been in demand for years [15,16,17,18,19,20]. In particular, radiative nuclear three-body capture processes are indispensable in bridging the $A = 5, 8$ gaps [17,21,22,23], but also building up the heavier nuclei may involve three-body reactions. Also, to pass the waiting points in the rapid proton capture process necessarily involves three particles, i.e. two protons and a core [24,25,19]. Along or outside the neutron dripline, or perhaps along the rapid neutron capture process, three particles may be involved as well in decay, capture, or reaction processes [12,8,26,27,28].

Traditionally, that is mostly for convenience of computation, the three-body reactions are described as two subsequent two-body reactions [15,21,16,29,19,30]. This two-step sequential mechanism has proved to be rather efficient in most cases but it cannot always be accurate. For

example, an intermediate configuration of some stability has to be present, and resonances offer themselves as these stepping stones. However, they may not be present or they may be too unstable, such that they decay too quickly after they are formed. It is also well-known that important contributions arise from the continuum background to the resonances [9,20,11]. This is often called the direct part. All such difficulties with the sequential models disappear by using the full three-body formulation of the reactions. Then the sequential mechanisms are still possible but now as a contributing process which does not have to be treated separately [31,30].

In reactions in stellar environments the temperature, rather than the energy, is often the parameter. For high temperature, if one of the two-body subsystems shows a relatively low-lying narrow resonance, the process is fairly accurately described by sequential model. In this case, although the three-body background contribution is missing in the description of the process, it is either small or appropriate parameter adjustments account for this part. When the intermediate two-body state is missing (or it is too broad), the strength function is continuous, without a significant peak structure arising from resonances [12,28], and the reactions can be described fairly well with knowledge of the three-body continuum and appropriate energy averaging [12,20,28].

At small temperature, where important astrophysical reactions take place, only very low energies are involved, which are typically clearly smaller than the energy of the

possible intermediate two-body states. As a consequence, the situation concerning the reaction mechanism is unclear. In any case, the complete computation of the direct process in coordinate space is very inaccurate due to the fact that a narrow grid of discrete continuum states is required in the very low energy region. This is often unaffordable from the numerical point of view, and the problem is usually achieved within the formalism by assuming a specific form of the strength function or equivalently of the photodissociation cross section [12, 20, 28]. This has the advantage of being a measurable quantity, and thus open to tests. To circumvent through pure theoretical calculations would require an accurate model and many points at small energies above the three-body threshold.

In view of the improved three-body techniques it is surprising that the sequential model still has not been systematically tested against genuine three-body computations. Even though such three-body results for small energies above threshold are inaccurate, it is still possible to compare direct and sequential rates by using the different model formulations with the same common input. This is the purpose of the present paper which focuses on the low temperature region such that only three-body energies below the intermediate two-body resonance energies are relevant for the reaction rate. For these temperatures reliability of the sequential model is more than dubious. The idea is to take the established and presently applied formulations for sequential capture, and compare to a similar formulation which includes the three-body direct capture. These calculations are based on the assumption of a specific form of the strength function (or the photodissociation cross section), and therefore do not require the precise numerical solution of the complicated three-body problem. Even though this is a drastic simplification of the problem, a comparison of the results obtained with the two possible mechanisms will permit to enlighten the importance of the direct capture mechanism at low temperature. In section II we give the appropriate definitions and formulae for later use. In section III we compute rates in the direct and sequential models and compare results as a function of the position and the widths of the two and three-body resonances. In section IV and V we apply the general method to the triple alpha process and the similar radiative capture leading to ${}^9\text{Be}$. Finally we summarize and conclude in section VI.

2 Direct versus sequential rates

A method computing the reaction rates for a three-body radiative capture reaction without assumptions about the underlying mechanism was employed previously in [12, 20, 28]. In the first part of this section we give a simplified description of this method, which, in particular, should be used when a direct capture takes place. However, when describing these processes, the corresponding reaction rates are traditionally described by a sequential mechanism via an intermediate structure [15, 16, 29, 21]. The main aspects of this description are summarized in the second part of

this section. By use of the different expressions given, a numerical comparison between both descriptions is allowed, in particular on the very low temperature region. This is done by use of the energy dependent penetration factors given in the last part of this section for each of the two possible capture mechanisms.

2.1 The direct picture

A three-body radiative capture process is usually denoted by $a + b + c \rightarrow A + \gamma$, and the reversed reaction is $A + \gamma \rightarrow a + b + c$, where a, b and c denote the three particles. The reaction rate at a given three-body kinetic energy E , $R_{abc}(E)$, can be obtained by use of Eqs.(20) and (32) in Ref. [15], which lead to:

$$R_{abc}(E) = \nu! \frac{\hbar^3}{c^2} \frac{8\pi}{(\mu_{ab}\mu_{ab,c})^{3/2}} \frac{2g_A}{g_a g_b g_c} \left(\frac{E_\gamma}{E}\right)^2 \sigma_\gamma(E_\gamma), \quad (1)$$

where $E_\gamma = E + |B|$ is the photon energy, B (< 0) is the three-body energy of the nucleus A , μ_{ab} and $\mu_{ab,c}$ are the reduced masses of the a - b two-body system (related to the Jacobi coordinate \mathbf{x}) and the ab - c system (related to the Jacobi coordinate \mathbf{y}), respectively [2], $g_i = 2J_i + 1$, where J_i is the angular momentum of particle i ($i = a, b, c, A$), and ν is the number of identical particles in the three-body system. Finally, $\sigma_\gamma(E_\gamma)$ is the photodissociation cross section of the nucleus A .

The energy averaged reaction rate is obtained as a function of the temperature T by using the Maxwell-Boltzmann distribution as weighting function. For three-particles the Maxwell-Boltzmann distribution takes the form:

$$B(E, T) = \frac{1}{2} \frac{E^2}{(k_B T)^3} e^{-\frac{E}{k_B T}}, \quad (2)$$

where k_B is the Boltzmann constant. We then obtain the following expression for the energy averaged reaction rate [12]:

$$\langle R_{abc}(E) \rangle = \nu! \frac{\hbar^3}{c^2} \frac{8\pi}{(\mu_{ab}\mu_{ab,c})^{3/2}} \frac{g_A}{g_a g_b g_c} \times \frac{1}{(k_B T)^3} \int_0^\infty E_\gamma^2 \sigma_\gamma(E_\gamma) e^{-\frac{E}{k_B T}} dE. \quad (3)$$

Therefore, once the photodissociation cross section σ_γ for the process $A + \gamma \rightarrow a + b + c$ is known, the rate $\langle R_{abc}(E) \rangle$ can be easily obtained. For instance, it can be obtained directly from the experimental σ_γ cross section.

Numerical calculation of σ_γ for the $A + \gamma \rightarrow a + b + c$ process is a delicate task, especially at low temperatures. For instance, the method used in [12, 20, 28] would require an extremely narrow grid of discrete continuum states. To achieve this, the continuum wave functions should be computed in a box of a sufficiently big size, which in turn would imply the need of an enormous basis set. All in all, the method becomes inefficient for such low temperatures. However, when the photodissociation proceeds by populating a three-body Breit-Wigner shaped resonance

of particles a , b , and c with total angular momentum J and energy E_R , then $\sigma_\gamma(E_\gamma)$ can be written as:

$$\sigma_\gamma(E_\gamma) = \frac{2J+1}{2g_A} \frac{\pi \hbar^2 c^2}{E_\gamma^2} \frac{\Gamma_{abc}(E) \Gamma_\gamma(E)}{(E - E_R)^2 + \Gamma(E)^2/4}, \quad (4)$$

where Γ_γ and Γ_{abc} are the partial decay widths of the resonance for gamma and three particle emission respectively, and $\Gamma = \Gamma_{abc} + \Gamma_\gamma$ is the total width. This is analogous to the method used in the usual sequential picture that is described in the next section. In this way, by using Eq.(4) the results provided by the two different schemes can be easily compared.

It is important to note that Eq.(3) has been derived without making any assumption concerning the reaction mechanism leading to the formation of the nucleus A . It is therefore completely general. In particular, this is the expression to be used when the capture mechanism is direct, meaning that the capture takes place without populating any intermediate two-body state. In this case the width $\Gamma_{abc}(E)$ corresponds to the width for direct decay of the three-body resonance into particles a , b , and c . For this reason we shall refer to Eq.(3) as the reaction rate in the “direct” or “three-body” picture.

2.2 The sequential picture

Let us now assume that one of the internal two-body subsystems, for instance the a - b system, shows a relatively narrow two-body resonance at some energy E_r . The usual procedure to understand reactions of the type $a + b + c \rightarrow A + \gamma$ is then to interpret it as two sequential two-body processes [16,29]. In the first step particle a captures b to populate the intermediate a - b two-body resonant state. In the second step, the a - b system is able, before decaying, to capture particle c , populate some three-body resonance of the nucleus A , and then decay by photo emission into one of the bound states of A .

The reaction rate for such a two-step process is given by the rate for the capture of c by the two-body subsystem a - b , $\langle R_{ab,c}(E'', E') \rangle$, weighted with the rate for formation of a - b [16]:

$$\langle R_{abc}(E'', E') \rangle = \frac{\nu!}{1 + \delta_{ab}} \frac{8\pi \hbar}{\mu_{ab}^2} \left(\frac{\mu_{ab}}{2\pi k_B T} \right)^{3/2} \int_0^\infty \frac{\sigma_{ab}(E'')}{\Gamma_{ab}(E'')} e^{-E''/k_B T} \langle R_{ab,c}(E'', E') \rangle E'' dE'', \quad (5)$$

where the total three-body energy, $E = E' + E''$, is given in terms of the relative energy, E'' , between particles a and b and the energy, E' , of particle c relative to the center of mass of a - b . The function δ_{ab} is 1 if a and b are identical particles, and 0 otherwise.

The elastic a - b cross section, σ_{ab} , in the equation above takes the form:

$$\sigma_{ab}(E'') = (1 + \delta_{ab}) \frac{g_{ab}}{g_a g_b} \frac{\pi}{\kappa^2} \frac{\Gamma_{ab}(E'')^2}{(E'' - E_r)^2 + (\Gamma_{ab}(E''))^2/4}, \quad (6)$$

where $\kappa^2 = 2\mu_{ab}E''/\hbar^2$, E_r is the energy of the resonance in the a - b system and $\Gamma_{ab}(E'')$ is the corresponding width, and $g_{ab} = 2J_{ab} + 1$, with J_{ab} being the angular momentum of the two-body resonance.

Also, following Ref.[16], we have that

$$\langle R_{ab,c}(E'', E') \rangle = \frac{8\pi}{\mu_{ab,c}^2} \left(\frac{\mu_{ab,c}}{2\pi k_B T} \right)^{3/2} \times \int_0^\infty \sigma_{ab,c}(E'', E') e^{-E'/k_B T} E' dE', \quad (7)$$

where the cross section $\sigma_{ab,c}(E'', E')$ for the capture of particle c by the two-body subsystem a - b is related to the photodissociation cross section through the detailed-balance (or reciprocity) theorem, which leads to [29]:

$$\sigma_{ab,c}(E') = \frac{g_A}{g_a g_b g_c} \frac{1}{\mu_{ab,c}} \frac{E_\gamma^2}{c^2 E'} \sigma_\gamma(E_\gamma), \quad (8)$$

where $E_\gamma = E + |B|$.

Similarly to the direct process, the photodissociation cross section σ_γ again takes the form:

$$\sigma_\gamma(E_\gamma) = \frac{2J+1}{2g_A} \frac{\pi \hbar^2 c^2}{E_\gamma^2} \frac{\Gamma_{ab,c}(E') \Gamma_\gamma(E' + E'')}{(E - E_R)^2 + \Gamma(E', E'')^2/4}. \quad (9)$$

This expression is formally identical to Eq.(4), but now $\Gamma_{ab,c}$ refers explicitly to the partial width for decay of the three-body resonance with angular momentum J into the two-body resonance a - b plus particle c . The assumption is that no other decay mode exists, and the direct decay circumventing this two-body path is not allowed, or at least negligibly small. As before, Γ_γ is then the partial width for gamma decay, and $\Gamma = \Gamma_{ab,c} + \Gamma_\gamma$ is the total width.

Replacement of Eq.(8) into (7), and of Eq.(7) into (5) leads then to the following expression for the energy averaged reaction rate:

$$\langle R_{abc}(E'', E') \rangle = \frac{\nu!}{1 + \delta_{ab}} \frac{g_A}{g_a g_b g_c} \frac{8\hbar}{\pi c^2 (k_B T)^3} \frac{1}{\mu_{ab}^{1/2} \mu_{ab,c}^{3/2}} \times \int_0^\infty E'' \frac{\sigma_{ab}(E'')}{\Gamma_{ab}(E'')} dE'' \int_{E''}^\infty E_\gamma^2 \sigma_\gamma(E_\gamma) e^{-E/k_B T} dE \quad (10)$$

where we have replaced the dependence on E' by E by use of $E = E' + E''$. We shall refer to the expression in Eq.(10) as the reaction rate in the “sequential” picture.

2.2.1 Extreme sequential limits

In this subsection we shall derive the form that the reaction rate (10) takes in the extreme cases of an infinitely narrow three-body resonance and/or an infinitely narrow intermediate two-body state. We shall refer to these rates as the ones obtained in the “extreme sequential” picture.

The connection between the reaction rates (3) and (10) is made evident for the particular case of a very narrow

a - b two-body resonance (Γ_{ab} very small compared to the energy of the resonance). In this case we have that Eq.(6) can be replaced by:

$$\frac{\sigma_{ab}(E'')}{\Gamma_{ab}(E'')} = (1 + \delta_{ab}) \frac{g_{ab}}{g_a g_b} \frac{2\pi^2}{\kappa^2} \delta(E'' - E_r), \quad (11)$$

from which Eq.(10) becomes:

$$\begin{aligned} \langle R_{abc}(E) \rangle &= \nu! \frac{\hbar^3}{c^2} \frac{8\pi}{(\mu_{ab}\mu_{ab,c})^{3/2}} \frac{g_A}{g_a g_b g_c} \times \\ &\times \frac{1}{(k_B T)^3} \int_{E_r}^{\infty} E_\gamma^2 \sigma_\gamma(E_\gamma) e^{-\frac{E}{k_B T}} dE. \end{aligned} \quad (12)$$

and the three-body energy E is given by $E_r + E'$.

We can immediately see that the reaction rates in Eqs.(3) and (12) are identical except for the lower limit in the integration. From 0 in the first case and from the intermediate two-body resonance energy E_r in the second. This reflects the fact that in the extreme sequential picture described by Eq.(12), where an infinitely narrow intermediate two-body resonance is assumed to be populated, the total three-body energy E must be larger than E_r . For three-body energies smaller than E_r this sequential picture cannot provide any decay, since the energy is too small to populate the two-body intermediate resonance. This means that in this extreme limit, when the three-body resonance energy E_R is smaller than E_r , the sequential decay has to proceed through the tail of the cross section in Eq.(9) corresponding to $E > E_r > E_R$.

We can also consider the case where the width $\Gamma_{ab,c}$ in Eq.(9) is very small. Assuming that $\Gamma_\gamma \ll \Gamma_{ab,c}$ is still fulfilled, we then have from Eq.(9) that:

$$\sigma_\gamma(E_\gamma) = \frac{2J+1}{g_A} \frac{\Gamma_\gamma(E) \pi^2 \hbar^2 c^2}{E_\gamma^2} \delta(E - E_R), \quad (13)$$

which leads to

$$\begin{aligned} \langle R_{abc}(E) \rangle &= \nu! \frac{2J+1}{g_a g_b g_c} \frac{(2\pi)^2 \hbar^5}{(k_B T)^3} \frac{\Gamma_\gamma(E_R)}{(\mu_{ab}\mu_{ab,c})^{3/2}} e^{-E_R/k_B T} \times \\ &\times \int_0^{E_R} \frac{\Gamma_{ab}(E'')}{(E'' - E_r)^2 + (\Gamma_{ab}(E''))^2/4} dE''. \end{aligned} \quad (14)$$

From the expression above we can see that when $E_R < E_r$ the decay in this limit must proceed through the tail of the cross section in Eq.(6) corresponding to $E'' < E_R < E_r$.

When the widths $\Gamma_{ab,c}$ and Γ_{ab} are both very small then the approximations (11) and (13) can be used simultaneously, and either Eq.(12) or (14) lead to the following expression for the energy averaged reaction rate:

$$\langle R_{abc}(E) \rangle = \nu! \frac{2J+1}{g_a g_b g_c} \frac{(2\pi)^3 \hbar^5}{(k_B T)^3} \frac{\Gamma_\gamma(E_R)}{(\mu_{ab}\mu_{ab,c})^{3/2}} e^{-E_R/k_B T} \quad (15)$$

which is valid when the two-body resonance energy E_r is below the three-body resonance energy E_R . Otherwise, if $E_R < E_r$ the reaction rate is zero in this limit of very small widths. The expression in Eq.(15) does not depend

on the energy E_r of the intermediate two-body resonance, and it is actually the same expression that one gets when the approximation (13) is used on the reaction rate (3) obtained in the direct picture.

At this point it is important to remind ourselves that Eqs.(12), (14), and (15) are limiting cases involving very, or even infinitely, narrow resonances. In particular, Eq.(12) permits to see very easily the connection between Eqs.(3) and (10). However, correct sequential calculations have to be performed by use of Eq.(10), as done for instance in [16] or [29].

2.3 Low energy dependence

The Boltzmann exponents in Eqs.(3) and (10) only allow contribution from three-body energies up to a few times $k_B T$. For instance, for a typical temperature in the core of a star of 10^7 K we have that $k_B T \approx 10^{-3}$ MeV, and only energies of the order of a few keV's and below can contribute to the rate. These energies are very small at the nuclear scale, where excitation energies are typically of the order of the MeV. Therefore, for such low temperatures, the reaction rate in Eq.(3) or (10) is dictated by the low energy tail of the corresponding cross sections.

As seen in Eqs.(4), (6), and (9) the behavior of the cross sections at very low energies is determined by the energy dependence of the partial widths, which are proportional to the penetration factor through the barrier responsible for the corresponding resonance ($\Gamma(E) \propto P(E)$). The constant of proportionality is determined by assuming that when evaluated at the resonance energy E_{res} the width $\Gamma(E_{res})$ provides the established (or experimental) width of the resonance Γ_0 . This is therefore leading to the expression:

$$\Gamma(E) = \Gamma_0 \frac{P(E)}{P(E_{res})}, \quad (16)$$

where the explicit form of the penetration factor $P(E)$ should be determined for each particular case.

For gamma decay it is well known from text books (see for instance the appendix E.1 of [32]) that the decay constant, and therefore the penetration factor and $\Gamma_\gamma(E)$, is proportional to $E_\gamma^{2\lambda+1}$, where $E_\gamma = E + |B|$ is the photon energy and λ is the multipolarity of the electromagnetic transition. As discussed in Eq.(16), the proportionality constant is determined in such a way that $\Gamma_\gamma(E_R)$ is equal to the experimental value Γ_γ for the gamma decay width. The parametrization is then:

$$\Gamma_\gamma(E) = \Gamma_\gamma \left(\frac{E + |B|}{E_R + |B|} \right)^{2\lambda+1}. \quad (17)$$

In the same way, when the Coulomb interaction is not involved, the partial widths $\Gamma_{ab,c}(E')$ and $\Gamma_{ab}(E'')$ in Eqs.(6) and (9) for the sequential picture take the form:

$$\Gamma_{ab,c}(E') = \Gamma_{ab,c} \left(\frac{E'}{E_R - E_r} \right)^{\ell_{ab,c}+1/2} \quad (18)$$

$$\Gamma_{ab}(E'') = \Gamma_{ab} \left(\frac{E''}{E_r} \right)^{\ell_{ab}+1/2}, \quad (19)$$

where $\ell_{ab,c}$ and ℓ_{ab} are the relative orbital angular momenta between particle c and the center of mass of a - b and between particles a and b , respectively, and where we have taken into account that the energy dependence of these partial widths is given by Eqs.(22) and (23) of Ref.[33].

When the Coulomb interaction is decisive, insertion of Eqs.(10) and (11) into (3) of Ref.[33] leads to the following energy dependence of the partial widths in the sequential picture:

$$\Gamma_{ab,c}(E') = \Gamma_{ab,c} \frac{1 + e^{2b_{ab,c}/\sqrt{E_R - E_r}}}{1 + e^{2b_{ab,c}/\sqrt{E'}}} \quad (20)$$

$$\Gamma_{ab}(E'') = \Gamma_{ab} \frac{1 + e^{2b_{ab}/\sqrt{E_r}}}{1 + e^{2b_{ab}/\sqrt{E''}}}, \quad (21)$$

where

$$b_{ab,c} = \frac{\pi}{2} (Z_a + Z_b) Z_c e^2 \sqrt{\frac{2\mu_{ab,c}}{\hbar^2}} \quad (22)$$

$$b_{ab} = \frac{\pi}{2} Z_a Z_b e^2 \sqrt{\frac{2\mu_{ab}}{\hbar^2}}, \quad (23)$$

and where Z_a , Z_b , and Z_c are the charges of particles a , b , and c , respectively, and e is the electron charge.

For direct decay we get, from Eqs.(12) and (3) of [33], for Coulomb potentials that:

$$\Gamma_{abc}(E) = \Gamma_{abc} \frac{1 + e^{2b_{abc}/\sqrt{E_R}}}{1 + e^{2b_{abc}/\sqrt{E}}} \quad (24)$$

with

$$b_{abc} = \frac{\pi}{2} \sqrt{\frac{2}{\hbar^2(m_a + m_b + m_c)}} \left(\sum (Z_i Z_j e^2)^{2/3} (m_i m_j)^{1/3} \right)^{3/2} \quad (25)$$

where m_a , m_b , and m_c are the masses of the particles and the sum runs over the three possible pairs of particles.

For direct decay, without Coulomb potentials, we get the energy dependence of $\Gamma_{abc}(E)$ in Eqs.(4) and (3) from Eq.(21) of Ref.[33]:

$$\Gamma_{abc}(E) = \Gamma_{abc} \left(\frac{E}{E_R} \right)^{\ell_{ab,c} + \ell_{ab} + 2}. \quad (26)$$

3 Parameter dependence

The computed reaction rates depend on the choice for the reaction mechanism, i.e. either direct or sequential. To illustrate it we start with a system of three identical charged particles. We shall assume that this three-body system has a resonance at the energy $E_R = 0.15$ MeV and $\Gamma_\gamma = 10^{-9}$ MeV. All the degeneracy factors g_i are taken equal to 1, the charges are taken twice the proton charge, and the masses equal to the mass of the alpha particle.

If the capture process is assumed to proceed directly, the reaction rate is then given by Eqs.(4) and (3), and

for three charged particles, the energy dependence of the width for particle decay is given by Eqs.(24) and (25). On the other hand, if we assume that the capture process takes place sequentially through an intermediate two-body resonance, the reaction rate is instead given by Eqs. (6), (9), and (10), and the energy dependence of the widths, Γ_{ab} and $\Gamma_{ab,c}$, for particle decay in Eqs.(6) and (9) are now as in (21) and (20).

As a first case, let us assume that the three-body and the intermediate two-body resonances are both narrow, e.g. by choosing $\Gamma_R = 10^{-5}$ MeV and $\Gamma_r = 10^{-6}$ MeV. The computed reaction rate in the direct picture is then given by the thick solid line in the upper part of Fig. 1. For the sequential case, when the capture proceeds through the intermediate two-body resonance, as seen in Eqs.(6) and (10), the reaction rate depends as well on the energy of the two-body resonance. We have chosen the energies of 0.05 MeV, 0.10 MeV, 0.13 MeV, and 0.20 MeV, as indicated by the straight lines in the right part of Fig 2. The straight line in the left part indicates the energy chosen for the three-body resonance. In this case of very narrow three-body and two-body resonances, the lorentzians describing them can not be distinguished from the lines indicating the energies in Fig. 2. The corresponding reaction rates in the sequential picture are given by the short-dashed, dot-dashed, and long-dashed curves in the upper part of Fig. 1 for the three cases where E_r takes the values 0.05 MeV, 0.10 MeV, and 0.13 MeV, respectively.

As we can see in the upper part of Fig. 1, for temperatures below about 0.02 GK the reaction rates in the two pictures differ from each other. In the first two cases, $E_r = 0.05$ MeV and $E_r = 0.10$ MeV, the sequential rate is below the direct one, while for $E_r = 0.13$ MeV, the sequential rate at low temperatures is above the direct one. This behavior is determined by the interplay between $\Gamma_{ab,c}$ and Γ_{ab} in Eqs.(20) and (21). When E_r increases and approaches E_R , then $\Gamma_{ab,c}$ increases, implying a more significant tail in the cross section (9), and therefore favoring an increase of the reaction rate at low temperatures. However, at the same time the increase of E_r decreases Γ_{ab} , which for the same reason tends to reduce the reaction rate. The final result of the competition between these two effects pushing in opposite directions depends on the masses and charges of the particles involved in the process. In our case the total effect amounts to an increase of the reaction rate when E_r increases. The comparison between the direct and the sequential calculations is better seen in the inner part of the figure, where the different curves show the ratio between the rates in the direct and sequential pictures. As we can see, the difference between them reaches up to 12 orders of magnitude for $T = 0.001$ GK.

For temperatures higher than about 0.03 GK the rates obtained in the sequential picture are not sensitive to the properties of the intermediate two-body resonance, and the computed rate agrees with the one obtained in the direct picture. This is consistent with the fact that when the three-body resonance and the two-body one are both very narrow the reaction rate can be approximated by Eq.(15),

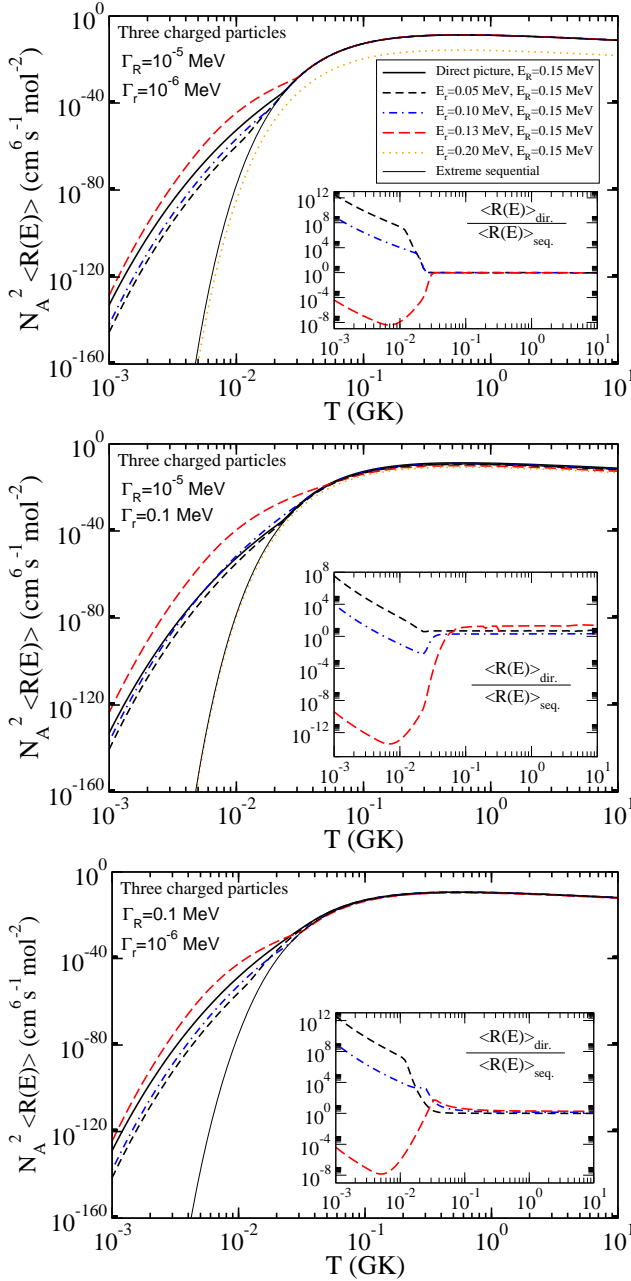


Fig. 1. (color online) Reaction rates for the radiative capture of three identical charged particles (with charge and mass equal to the ones of the α -particle). The widths Γ_R and Γ_r of the three- and two-body resonances are 10^{-5} MeV and 10^{-6} MeV, respectively in the upper part, 10^{-5} MeV and 0.1 MeV, respectively in the central part, and 0.1 MeV and 10^{-6} MeV, respectively in the lower part. The thick-solid curve shows the reaction rate in the direct picture. The short-dashed, dot-dashed, and long-dashed curves are the rates in the sequential picture for two-body energies $E_r = 0.05$ MeV, 0.10 MeV, and 0.13 MeV. The ratio between the rates in the direct and sequential pictures are shown in the insets. The thin solid line is the rate in the extreme sequential limit. The dotted curve is the reaction rate obtained when $E_r = 0.20$ MeV ($E_R < E_r$) (see text). N_A is the Avogadro's number.

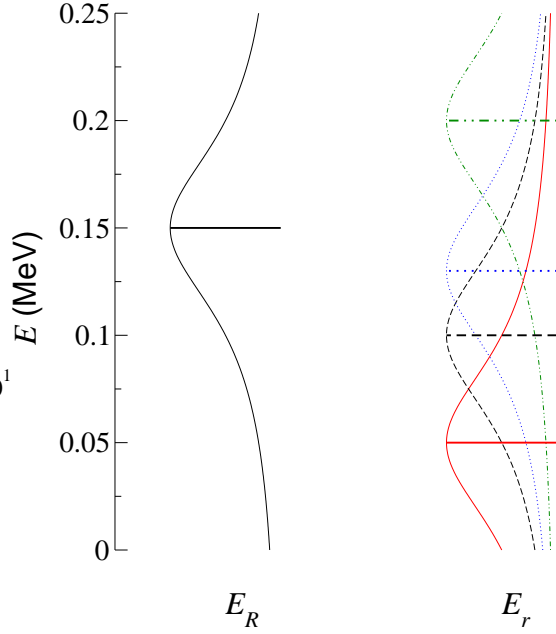


Fig. 2. (color online) Energy diagram showing the three-body resonance energy E_R and two-body resonance energies E_r used in the schematic calculations in section III. The curves are the lorentzians corresponding the resonances when having a width of 0.1 MeV.

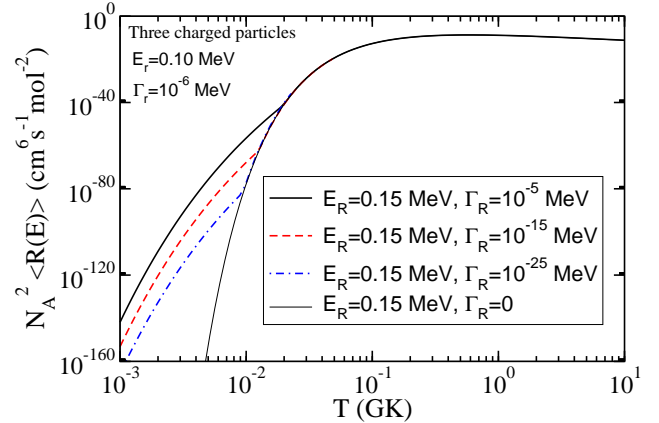


Fig. 3. (color online) Reaction rates in the sequential picture for the same system as in the upper part of Fig. 1 with $E_r = 0.10$ MeV but for different small values for the width of the three-body resonance Γ_R . The thick-solid and thin-solid curves are the same as the dot-dashed and thin-solid curves in the upper part of Fig. 1. The dashed and dot-dashed curves are calculations with $\Gamma_R = 10^{-15}$ MeV and $\Gamma_R = 10^{-25}$ MeV, respectively.

which depends neither on E_r nor on Γ_r . This is referred to as the rate in the extreme sequential picture, and it is shown in the upper part of Fig. 1 by the thin solid line. As we can see, for $T \gtrsim 0.03$ GK this approximation agrees with both the full direct and the sequential calculations. At low temperatures this is not true anymore, which shows that the finite width of the resonances influences the rates, and the limit of zero width leading to

Eq.(15) becomes increasingly invalid. The reason is that the effect from the tails of the resonances, where the penetration factors play a role, is completely absent in Eq.(15). This is easily recognized in Fig. 3, where the thick-solid and thin-solid curves are the same as the dot-dashed and thin-solid ones in the upper part of Fig. 1 (sequential reaction rate with $E_r = 0.10$ MeV and reaction rate in the extreme sequential limit, respectively), while the dashed and dot-dashed curves are the calculations with $\Gamma_R = 10^{-15}$ MeV and $\Gamma_R = 10^{-25}$ MeV, respectively. As we can see, the narrower the three-body resonance the lower the temperature at which the full sequential calculation matches the curve in the extreme sequential picture.

The central and lower parts of Fig. 1 show the same reaction rates as in the upper part, but for $\Gamma_r = 0.1$ MeV and $\Gamma_R = 0.1$ MeV, respectively. A feeling of the overlap between the three-body and two-body resonances in the different cases can be got from Fig. 2, where the curves plotted are lorentzians with $\Gamma = 0.1$ MeV. The behavior observed in the central and lower parts of Fig. 1 is similar to the one found in the upper part, where both resonances are simultaneously narrow. Also the ratio between the direct and sequential calculations (inner part of the figures) is similar. In these two cases, the extreme sequential curves correspond to the ones obtained with the expressions (14) and (12), respectively. As we can see, Eq.(14) does actually depend on the properties of the two-body resonance energy, which leads in this case (central part of Fig. 1) to some small differences between the different calculations. In particular, the curve in the figure (thin solid line) has been obtained using $E_r = 0.10$ MeV.

It is important to note that the equations in Ref.[33] which have led to Eqs.(18) and (21) have been obtained using the adiabatic approximation to describe the three-body system. The penetration factors are then extracted from the WKB tunneling probability through the potential barrier of the lowest adiabatic potential. When one of the two-body systems has a resonance, this lowest adiabatic potential shows a flat region at the two-body resonance energy, and eventually goes to zero. The narrower the two-body resonance, the longer its lifetime, and the larger the flat region in the adiabatic potential. In fact, in the limit of zero width (or infinite lifetime) we actually have a bound two-body state, and the adiabatic potential goes asymptotically to the two-body energy of the bound state. This implies that the expressions (18) and (20) are meaningful only when the three-body resonance energy E_R is bigger than the two-body resonance energy E_r .

In the opposite case, when $E_R < E_r$, the reaction mechanism is dominantly direct, since the intermediate configuration is energetically forbidden. However, it is still possible to exploit the sequential mechanism but obviously not until the decay is completed. The distance between particles must be limited, or equivalently the time allowed for the non-energy conserving process is limited. If the decay still has to take place through the sequential decay mechanism then the two-body resonance width has to be finite (see the dot-dashed curve in Fig. 2, where even if it corresponds to $E_R < E_r$ a significant part of the reso-

nance tail falls in the energetically allowed region). This mechanism was previously named virtual sequential decay [25].

From the discussion above we then have that, when $E_R < E_r$, the barrier determining the penetration factor is much bigger than in the opposite case, and in fact the narrower the two-body resonance the thicker the barrier. As a consequence, for $E_R < E_r$ we have that Eqs.(18) and (20) can not be used, and the three-body width is expected to be much smaller than when $E_R > E_r$. For this reason, the reaction rate for the cases where $E_R < E_r$ can only be estimated from Eq.(14), where the value of $\Gamma_{ab,c}$ has been assumed to be zero. From this equation, since $E_R < E_r$, we can immediately see that the reaction rate is produced by the tail of the intermediate two-body resonance (dot-dashed curve in Fig. 2). Clearly, the broader this resonance the larger the reaction rate. This is shown by the dotted curves in the upper and central parts of Fig. 1 for $\Gamma_r = 10^{-6}$ MeV and $\Gamma_r = 0.1$ MeV, respectively. These two calculations have been made with resonance energies $E_r = 0.20$ MeV and $E_R = 0.15$ MeV.

In the central part the width of the two-body resonance is not small, $\Gamma_r = 0.1$ MeV, and the difference with the previous calculations is hardly seen in logarithmic scale, although it is two orders of magnitude smaller than the direct picture calculation. When $\Gamma_r = 10^{-6}$ (upper part), the dotted curve is up to eight orders of magnitude smaller than the other calculations, consistent with the fact that in the limit where $\Gamma_r = 0$ the rate provided by Eq.(12) is zero. In the lower part of the figure the corresponding calculation with $E_r = 0.20$ MeV is not shown. First, because for $E_R < E_r$ the width of the three-body resonance is expected to be very small, which is not the case in this calculation, and second, because even if we insist in computing it, the penetration factors (18) and (20) are obviously meaningless for $E_R < E_r$, and another parametrization would have to be designed.

For completeness, we show in Figs. 4 and 5 the same calculations as in Fig. 1, but only for the cases where, respectively, two or none of the particles forming the two-body resonance are charged. The meaning of the curves is as in Fig. 1, and the only difference lies in the use of the proper penetration factors for the cases where the Coulomb interaction can be neglected.

In particular, in Fig. 4 we assume that the two charged particles are the ones forming the intermediate two-body resonance in the sequential picture. Therefore, the penetration factors to be used are (24) in the direct case, and (18) and (21) in the sequential case. In this case, when E_r increases and approaches E_R we have that $\Gamma_{ab,c}$ increases as a polynomial, while Γ_{ab} decreases exponentially. As a consequence, the decrease in the reaction rate due to the decrease of Γ_{ab} dominates over the increase produced by the increase of $\Gamma_{ab,c}$, and the final result is that the computed reaction rate decreases at low temperatures when E_r increases, although the difference between the calculations when $E_r = 0.10$ MeV and $E_r = 0.13$ MeV is hardly seen in the figure. In Fig. 5 the penetration factors to be used are (26) in the direct case, and (18) and (19) in the

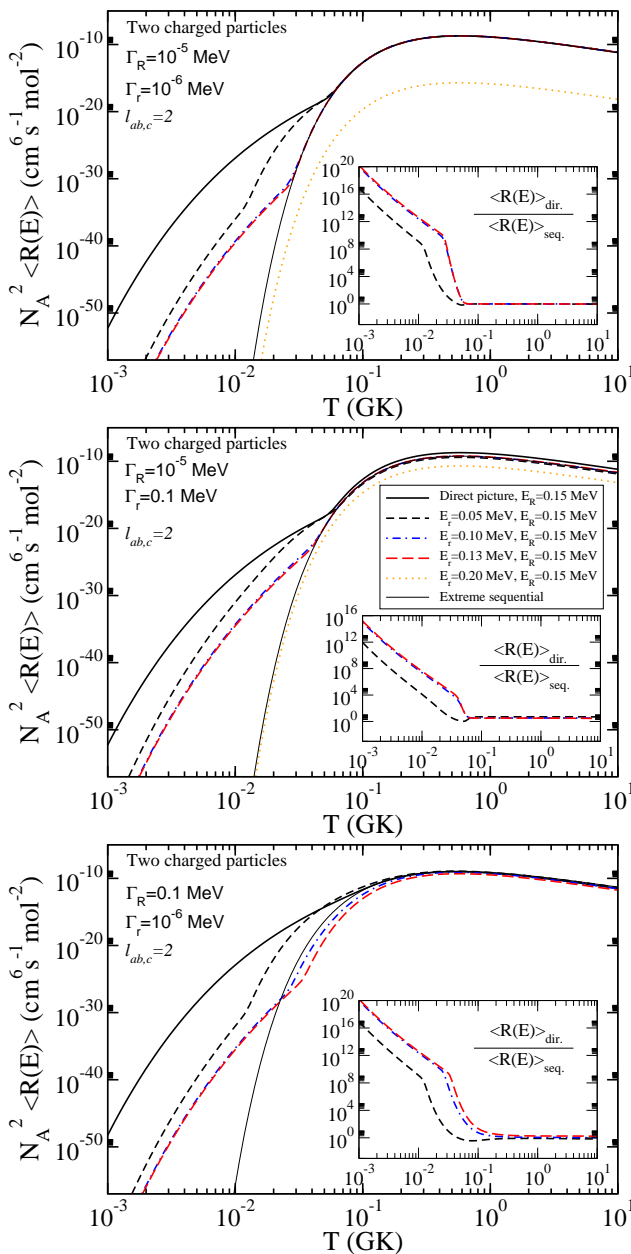


Fig. 4. (color online) The same as in Fig. 1 when only the two particles forming the intermediate two-body resonance are charged. The centrifugal barriers correspond to orbital angular momentum $\ell_{ab,c} = 2$.

sequential case. The general trends of the reaction rates shown in Figs. 4 and 5 are similar to the ones shown and discussed in Fig. 1. The main difference is the absolute value of the rates at small temperatures, which increases enormously when the Coulomb barrier disappears.

These general features of the reaction rates, especially the ones concerning their dependence on model assumptions of the capture process, can now be used in practical cases of (astro)physical interest. We shall in the next two sections focus on the triple alpha reaction (three identical charged particles with narrow three-body and intermediate two-body resonances), and on the $\alpha + \alpha + n \rightarrow {}^9\text{Be} + \gamma$

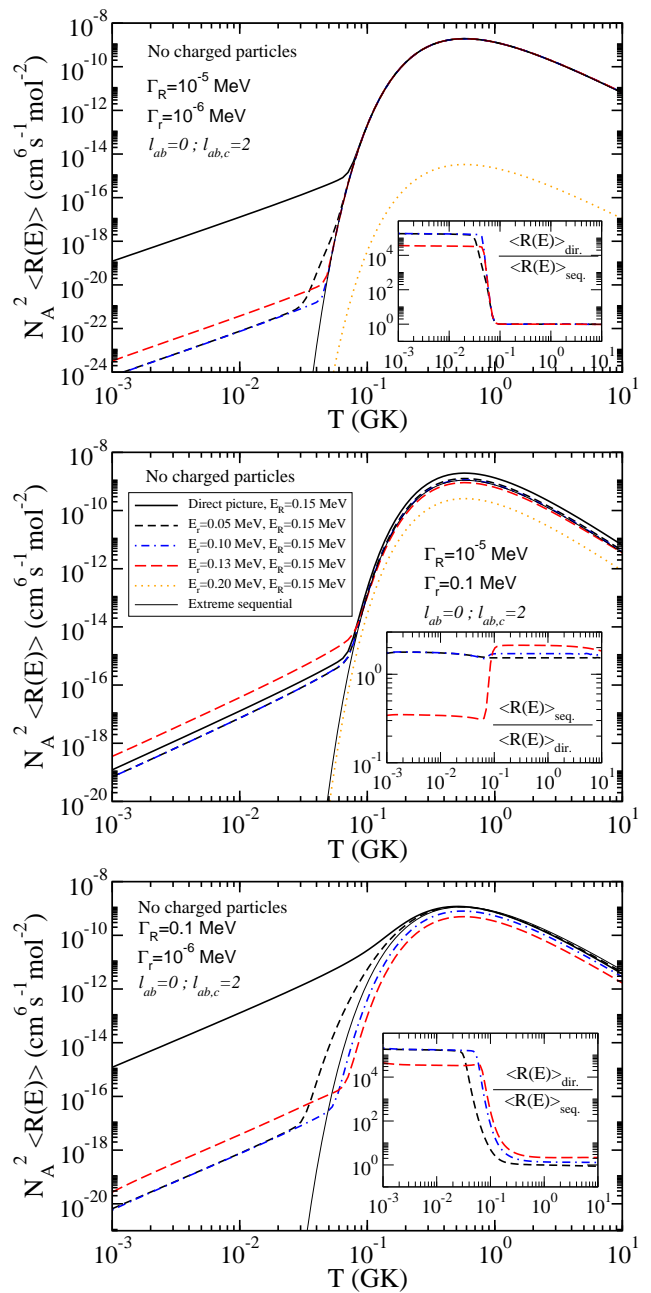


Fig. 5. (color online) The same as in Fig. 1 for three identical uncharged particles. The centrifugal barriers correspond to orbital angular momentum $\ell_{ab,c} = 2$.

process (two identical charged particles forming a narrow two-body resonance, and a relatively broad three-body resonance).

4 The triple alpha rate

The reaction rate for the triple alpha reaction, $\alpha + \alpha + \alpha \rightarrow {}^{12}\text{C} + \gamma$, at very low temperatures is quite controversial. In fact, in the recent work [34], the reaction rate at a temperature of 10^{-2} GK has been found to be about 20 orders

of magnitude bigger than the one given in the NACRE compilation [16]. Such enormous increase in the reaction rate would have dramatic consequences for the late stages of the stellar evolution in low mass stars [35].

As demonstrated in the previous sections, the key quantity to obtain an accurate reaction rate for a radiative capture process is the photodissociation cross section for the inverse reaction. This means that in our case σ_γ for the $^{12}\text{C}+\gamma \rightarrow \alpha+\alpha+\alpha$ reaction is needed. This cross section is, to a large extent, determined by the resonance spectrum in ^{12}C , which is rather well known except for the lowest 2^+ resonance, whose excitation energy is not well established yet. Fortunately, as shown in [20], this resonance is playing a role in the reaction rate only for temperatures higher than about 2 GK. Therefore, this uncertainty in the ^{12}C spectrum is irrelevant for the analysis of the reaction rate at very low temperatures, which is dominated by the E2 transition $0^+ \rightarrow 2_1^+$ [20]. This notation defines the transitions from the 0^+ continuum states in the three α system to the bound 2^+ state in ^{12}C .

Furthermore, as also shown in [20], for temperatures higher than 0.1 GK the computed contribution to the reaction rate from the $0^+ \rightarrow 2_1^+$ transitions is very similar when performing a full three-body calculation and when assuming a sequential capture through the low-lying 0^+ state in ^8Be (0.092 MeV above the two-body threshold). This is due to the existence of the narrow 0^+ Hoyle three-body resonance in ^{12}C at about 0.38 MeV above threshold. This state heavily dominates the calculation, which has a large strength corresponding to strong population and subsequent decay of the Hoyle state. Three-body calculations have shown that the particle decay of the Hoyle state proceeds almost fully sequentially [36], and therefore so does also the inverse process.

However, for very small temperatures the relevant three-body energies in the reaction rate are clearly below the 0.092 MeV of the intermediate 0^+ resonance in ^8Be . It is then not so obvious that the sequential picture through that 0^+ state is still appropriate. The occurrence of a direct or a sequential capture mechanism would imply a different behavior of the tail of the photodissociation cross section (see Eqs.(20) and (24)), and therefore it would lead to a different reaction rate. This is in fact observed in the schematic case in the upper part of Fig. 1, where an example similar to the triple alpha reaction showed a model dependent rate varying by several orders of magnitude at low temperatures.

4.1 The photodissociation cross section

As mentioned above, for temperatures higher than 0.1 GK the direct and sequential descriptions provide similar results. Therefore, for $T > 0.1$ GK, the simplest choice for the photodissociation cross section of ^{12}C is the sequential expression given by Eq.(9). We use the same values for the energies and widths of the different states in ^{12}C and ^8Be as the ones specified in [16]. The energy dependence of the widths is then as given by Eq.(17) (with $\lambda = 2$) for $\Gamma_\gamma(E)$,

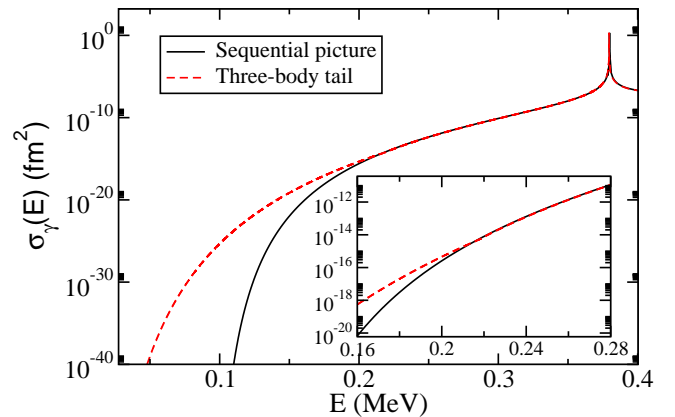


Fig. 6. (color online) Photodissociation cross section as given in Eq.(9) for the $^{12}\text{C}+\gamma \rightarrow \alpha+\alpha+\alpha$ reaction as a function of the three-body energy E . The parameters are as given in [16]. The solid line has been obtained assuming a sequential mechanism, using the widths as given in (20) and (22). The dashed line corresponds to a direct mechanism, using the widths as given in (24) and (25). The inner part is a zoom of the cross section in the matching region.

and as given by Eq.(20) (with the b -parameter (22)) for $\Gamma_{ab,c}(E)$.

If we now assume that the same energy dependence, corresponding to a sequential mechanism, is still valid for low energies, we then get the photodissociation cross section shown by the solid line in Fig. 6. The peak at about 0.38 MeV corresponds to the Hoyle state.

The other possibility is that at low energies the photodissociation cross section be dominated by a direct process. In this case the tail of the cross section would be given by Eq.(24), where the b -parameter is now as in Eq.(25). Then Eq.(4) leads to the cross section shown by the dashed line in Fig. 6. The tail of the photodissociation cross section matches well with the one in the sequential picture (solid line) at about 0.2 MeV, as seen in the inner part of the figure.

As we can see, for three-body energies smaller than 0.2 MeV the dashed and solid curves are very different. Although still small in absolute values, the cross section in the direct picture (dashed line) can be orders of magnitude bigger than the one in the sequential picture (solid line). This difference is necessarily giving rise to different reaction rates at small temperatures. How sizable the difference is between the reaction rates is the topic of the following subsection.

4.2 Reaction rates

In Fig. 7 the solid and open circles are the reaction rates for the triple alpha reaction given by Fowler et al. in Ref.[15] and the NACRE compilation [16], respectively. The main difference between these rates is found at high temperatures, where the result from [15] is below the one of NACRE [16]. This is due to the fact that while the effects of the first 2^+ resonance are included in [16], they are

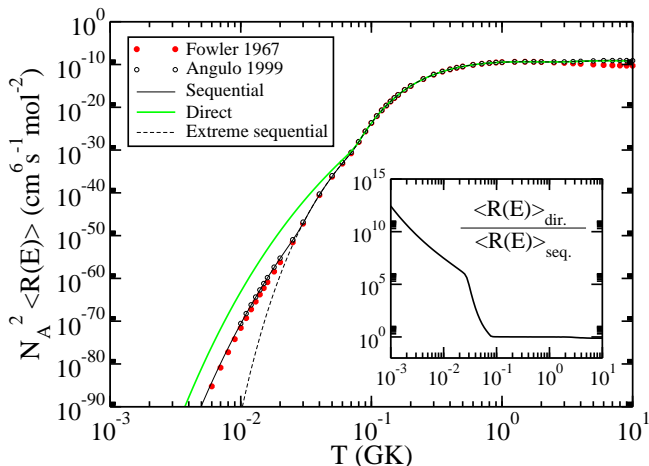


Fig. 7. (color online) Reaction rate for the triple α process. The solid and open circles are the results from [15] (Fowler 1967) and [16] (Angulo 1999), respectively. The thick solid curve is the calculation as in Eq.(3) assuming a direct capture process at very low energies. The thin solid line is the calculation in the sequential picture (10). The dashed line has been obtained in the extreme sequential approximation (12). The inset shows the ratio between the thick solid rate (direct capture assumption at low energies) and the thin solid line (sequential capture assumption at low energies).

omitted in [15]. At low temperatures, both calculations, assuming both a fully sequential capture mechanism, provide essentially the same result. In the calculations shown in this section the lowest 2^+ resonance in ^{12}C has been included using the resonance parameters given in [16].

In the figure, the thin dashed line gives the reaction rate obtained in the extreme sequential model, i.e., when Eq.(9) (solid curve in Fig. 6) is inserted into Eq.(12). This approximation amounts to cutting the tail of the cross section for energies smaller than the one of the intermediate 0^+ state in ^8Be . This strong approximation gives rise to a reaction rate in good agreement with the results in [15] and [16] at high temperatures, while for temperatures smaller than ~ 0.03 GK it clearly underestimates the rate. This is consistent with Fig. 3, where we see that a decreasing width of the three-body resonance increases the range of temperatures where the sequential and the extreme sequential calculations agree.

A full sequential description of the process requires the use of Eq.(10). Compared to the extreme sequential limit, this calculation includes now the low energy tails of the cross sections (6) and (9), which are given by (21) and (20), respectively. This is done in [16], and since we are using the same resonance parameters, we of course recover the same result (thin solid line in the figure).

However, when the low energy tail in σ_γ is assumed to be given by (24), which corresponds to a direct capture (dashed curve in Fig. 6), and the σ_γ cross section (4) is inserted into Eq.(3), we then get the reaction rate shown by the thick solid line in Fig. 7. As we can see, for temperatures smaller than ~ 0.07 GK, the reaction rate obtained assuming a direct capture at very low energies is several

T (GK)	Reaction Rate (cm ⁶ s ⁻¹ mol ⁻²)		
	Direct	Sequential	Ref.[16] (adopted)
0.001	4.50×10^{-144}	1.64×10^{-156}	—
0.002	4.97×10^{-113}	1.14×10^{-123}	—
0.003	5.47×10^{-98}	1.02×10^{-107}	—
0.004	1.64×10^{-88}	1.20×10^{-97}	—
0.005	8.99×10^{-82}	1.77×10^{-90}	—
0.006	1.23×10^{-76}	5.26×10^{-85}	—
0.007	1.54×10^{-72}	1.25×10^{-80}	—
0.008	3.71×10^{-69}	5.12×10^{-77}	—
0.009	2.66×10^{-66}	5.83×10^{-74}	—
0.01	7.67×10^{-64}	2.52×10^{-71}	2.93×10^{-71}
0.02	1.09×10^{-49}	4.65×10^{-56}	5.45×10^{-56}
0.03	7.90×10^{-43}	8.20×10^{-48}	1.46×10^{-47}
0.04	1.71×10^{-38}	3.16×10^{-41}	5.31×10^{-41}
0.05	2.15×10^{-35}	6.68×10^{-37}	1.04×10^{-36}
0.06	5.19×10^{-33}	8.16×10^{-34}	1.20×10^{-33}
0.07	4.92×10^{-31}	2.18×10^{-31}	3.00×10^{-31}
0.08	8.84×10^{-29}	7.82×10^{-29}	9.68×10^{-29}
0.09	2.22×10^{-26}	2.12×10^{-26}	2.52×10^{-26}
0.10	2.11×10^{-24}	2.04×10^{-24}	2.38×10^{-24}

Table 1. Computed reaction rates for the $\alpha + \alpha + \alpha \rightarrow ^{12}\text{C} + \gamma$ reaction assuming a direct capture for the low energy tail of σ_γ (second column) and assuming a fully sequential process (third column). The fourth column gives the adopted reaction rate given in the NACRE compilation [16].

orders of magnitude bigger than when the sequential capture is assumed. This is appreciated more quantitatively in the inset of the figure, where we show the ratio between both reaction rates, direct and sequential. We can immediately see that the ratio increases when decreasing the temperature. For a temperature of 10^{-3} GK we have obtained a reaction rate for the direct capture about 12 orders of magnitude bigger than in the sequential picture. This difference reduces to about 7 orders of magnitude for $T=0.01$ GK.

In table 1 we give the computed reaction rates in the direct picture (second column) and in the sequential picture (third column) for temperatures from 10^{-3} GK to 0.1 GK. In Ref.[16] a lower limit, a higher limit, and an adopted value are given for this reaction rate. Our results in the sequential approach lie in between the two limits given in [16], although closer to the lower one. In the last column of table 1 we give the reaction rates quoted in Ref.[16] as adopted rate.

It is important to note that the computed rates are the ones obtained in the limiting cases of a fully direct or a fully sequential description in the very low energy region. If both processes compete, the computed reaction rate would then be found in between the thin and thick solid curves in Fig. 7, which can be taken as the upper and lower limits to the true reaction rate. In any case, even if the process is considered to be fully direct, the increase in the reaction rate compared to the NACRE result at $T=0.01$ GK is of only 7 orders of magnitude (see table 1), and thus far smaller than the 20 orders of magnitude obtained in [34].

We emphasize that the calculation in the direct picture has been made with the same value of Γ_γ ($= 3.7 \times 10^{-3}$ eV) as in the sequential picture. A change in Γ_γ implies precisely the same change in the reaction rate, as seen immediately from Eqs.(4) and (3).

5 The ${}^9\text{Be}$ rate

Let us consider the $\alpha + \alpha + n \rightarrow {}^9\text{Be} + \gamma$ reaction where the principles are similar to the case of ${}^{12}\text{C}$. The properties of the low energy spectrum of ${}^9\text{Be}$ will determine the reaction rate at low temperatures. As for ${}^{12}\text{C}$, the presence of the internal two-body subsystem, ${}^8\text{Be}$ with the very narrow 0^+ resonance at 0.092 MeV, suggests a sequential description of the capture process as the most appropriate model [16, 29].

The main difference compared to ${}^{12}\text{C}$ is that now ${}^9\text{Be}$ does not show a low-lying and narrow three-body resonance like the Hoyle state. Instead, ${}^9\text{Be}$ has a low lying $1/2^+$ resonance in the vicinity of 0.11 MeV [37], only slightly above the 0.092 MeV of the 0^+ resonance in ${}^8\text{Be}$. The width of the $1/2^+$ state is estimated to be around 0.1 MeV, although 0.2 MeV is not numerically excluded [38]. As a consequence the photodissociation cross section shows a relatively broad peak at a three-body energy of around 0.11 MeV, in such a way that σ_γ is not negligible in the vicinity of the two-body resonance energy $E_r = 0.092$ MeV. The system under investigation is now similar to the schematic case shown in the lower part of Fig. 4.

5.1 The photodissociation cross section

The experimental photodissociation cross section of ${}^9\text{Be}$ can be found in [29], and it is shown in Fig. 8 by the solid circles as a function of the three-body energy E . Very recently new data for the peak corresponding to the $1/2^+$ resonance in ${}^9\text{Be}$ have been published in [39], and they are shown by the open circles in the figure. The experimental data show that for three-body energies below the 0^+ resonance at 0.092 MeV in ${}^8\text{Be}$, the cross section essentially vanishes, or at least it is extremely small. The energy of the two-body 0^+ resonance is indicated by the arrow on the x -axis.

This fact supports the assumption that the intermediate 0^+ state in ${}^8\text{Be}$ is actually populated in the process, and therefore the sequential description appears to be appropriate. In fact, the energy dependence of the cross section (9) for sequential decay of ${}^9\text{Be}$ into ${}^8\text{Be}$ plus a neutron is governed by (18), which implies that σ_γ vanishes when $E' = 0$, i.e., when $E = E_r$. Furthermore, for high temperatures, a pure three-body calculation of the reaction rate, without any additional assumption about the reaction mechanism, agrees reasonably well with the one obtained in the sequential picture [12].

As for ${}^{12}\text{C}$, the behavior of σ_γ at very low energies, where again σ_γ takes very small values, will determine the value of the reaction rate at very low temperatures, and this rate could change depending on which model, direct or

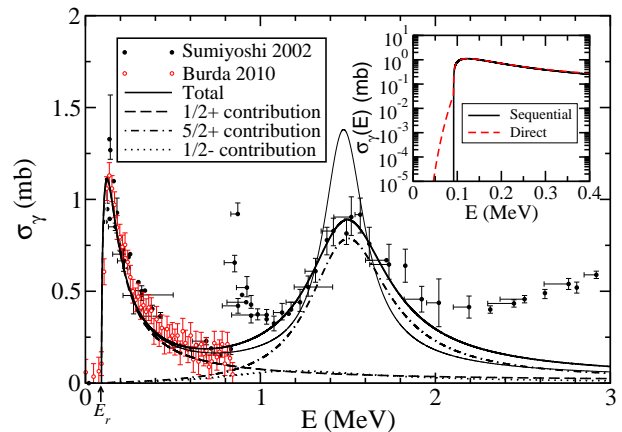


Fig. 8. (color online) Photodissociation cross section for ${}^9\text{Be}$ as a function of the three-body energy E . The experimental data are from [29] (Sumiyoshi 2002, solid circles) and from [39] (Burda 2010, open circles). The dashed, dot-dashed, and dotted curves correspond to the contribution of the $1/2^+$, $5/2^+$, and $1/2^-$ states in ${}^9\text{Be}$, respectively. The thick solid line gives the sum of the three contributions. The $5/2^+$ resonance is fitted as in [29]. The solid thin line is the total cross section when the $5/2^+$ resonance is parametrized as in [16]. The vertical arrow in the x -axis indicates the energy of the 0^+ resonance in ${}^8\text{Be}$. The inner part is a zoom of the low energy region of the cross section, where the solid and dashed lines are the cross section when the sequential and direct pictures are assumed in the low energy region, respectively.

sequential, is assumed for the capture mechanism at such low energies. To investigate this issue we proceed as for ${}^{12}\text{C}$. At high temperatures the three-body and sequential pictures provide similar results (as we can see in the lower part of Fig. 4). For energies higher than E_r we then start by taking the simple parametrization of the cross section used in the sequential description. In particular, we again choose the resonance parameters given in [16], and the $1/2^+$, $5/2^+$, $1/2^-$ resonances in ${}^9\text{Be}$ are included in the calculation. This gives rise to the cross section shown in Fig. 8 by the thin solid line, where the energy dependence given by Eq.(17) with $\lambda = 1$, and Eq.(18), has been used for all the resonances.

The peak corresponding to the $5/2^+$ resonance is clearly overestimated. To solve this problem, we have taken for this particular ${}^9\text{Be}$ resonance the energy and width used in [29], which gives a much better agreement with the experimental cross section, as shown by the thick solid line. In any case, the properties of the $5/2^+$ resonance play a minor role in the low temperature behavior of the reaction rate. The relevant resonance in this temperature region is the $1/2^+$ state, for which similar parameters are employed in [16] and [29]. In Fig. 8 the dashed, dot-dashed, and dotted curves show the contribution to the total cross section (thick solid curve) from the $1/2^+$, $5/2^+$, and $1/2^-$ resonances, respectively.

In the inner part of Fig. 8 we show a zoom of the low energy region of the photodissociation cross section. When the sequential picture is assumed, the cross section takes the form (9) with $\Gamma_{ab,c}$ given by (18), and then σ_γ

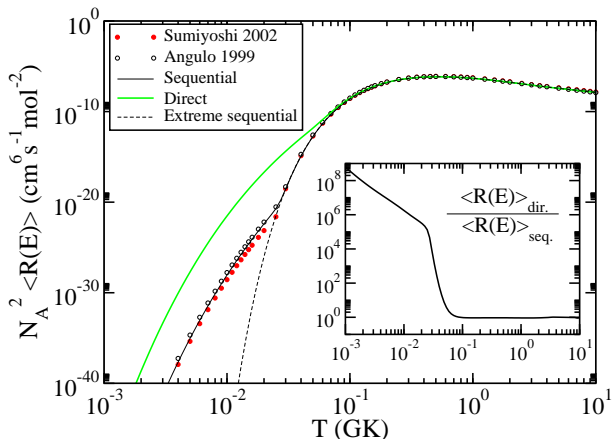


Fig. 9. (color online) Reaction rate for the reaction $\alpha + \alpha + n \rightarrow {}^9\text{Be} + \gamma$. The solid and open circles are the results from [29] (Sumiyoshi 2002) and [16] (Angulo 1999), respectively. The dashed line has been obtained in the extreme sequential approximation (12). The thin solid line is the calculation in the sequential picture (10). The thick solid curve is the calculation (3) assuming a direct capture process at very low energies (dashed curve in the inset of Fig. 8). The inset shows the ratio between the thick solid rate (direct capture assumption at low energies) and the thin solid line (sequential capture assumption at low energies).

vanishes for $E = E_r$, as shown by the solid line in the inset of the figure. However, if for such low energies we assume a direct mechanism, due to the Coulomb repulsion of the two alpha particles, the low energy behavior of the cross section takes the form (24), and the cross section behaves as shown by the dashed line in the inset of Fig. 8.

5.2 Reaction rates

The solid and open circles in Fig. 9 are the reaction rates for the $\alpha + \alpha + n \rightarrow {}^9\text{Be} + \gamma$ process given by Sumiyoshi et al. in Ref.[29] and the NACRE compilation [16], respectively. They basically agree in the whole temperature range shown in the figure, although for low temperatures the results from [29] are slightly below the ones in [16]. This is due to the fact that the treatment of the low energy tails in the cross section is not exactly the same in both cases. More precisely, for the $5/2^+$ resonance the widths involved in Eqs.(6) and (9) are taken as constant in [16], while in [29] they are assumed to be energy dependent. In the present work we use the same energy dependence as for the $1/2^+$ resonance, and therefore our computed reaction rates in the sequential picture at very low temperatures should also be a bit smaller than the ones given in [16].

If we now take the cross section given by the thick solid line in Fig. 8 and use it in Eq.(12), we then get the reaction rate in the extreme sequential picture, which is shown by the dashed line in Fig. 9. As expected, this crude approximation fails completely at low temperatures. As we already know, a correct sequential calculation requires use

T (GK)	Reaction Rate (cm ⁶ s ⁻¹ mol ⁻²)		
	Direct	Sequential	Ref.[16] (adopted)
0.001	2.35×10^{-50}	9.00×10^{-60}	3.90×10^{-59}
0.002	2.25×10^{-39}	7.62×10^{-48}	2.50×10^{-47}
0.003	4.30×10^{-34}	4.76×10^{-42}	1.35×10^{-41}
0.004	8.80×10^{-31}	2.18×10^{-38}	5.58×10^{-38}
0.005	1.94×10^{-28}	8.93×10^{-36}	2.11×10^{-35}
0.006	1.17×10^{-26}	8.84×10^{-34}	1.96×10^{-33}
0.007	3.06×10^{-25}	3.50×10^{-32}	7.39×10^{-32}
0.008	4.48×10^{-24}	7.33×10^{-31}	1.48×10^{-30}
0.009	4.30×10^{-23}	9.66×10^{-30}	1.88×10^{-29}
0.01	3.00×10^{-22}	8.96×10^{-29}	1.69×10^{-28}
0.02	1.99×10^{-17}	4.10×10^{-23}	6.29×10^{-23}
0.03	4.14×10^{-15}	2.85×10^{-19}	5.05×10^{-19}
0.04	1.21×10^{-13}	1.20×10^{-15}	1.90×10^{-15}
0.05	1.51×10^{-12}	1.76×10^{-13}	2.58×10^{-13}
0.06	1.29×10^{-11}	4.66×10^{-12}	6.44×10^{-12}
0.07	8.03×10^{-11}	4.64×10^{-11}	6.14×10^{-11}
0.08	3.54×10^{-10}	2.52×10^{-10}	3.24×10^{-10}
0.09	1.16×10^{-9}	9.17×10^{-10}	1.15×10^{-9}
0.10	3.02×10^{-9}	2.53×10^{-9}	3.12×10^{-9}

Table 2. Computed reaction rates for the $\alpha + \alpha + n \rightarrow {}^9\text{Be} + \gamma$ reaction assuming a direct capture for the low energy tail of σ_γ (second column) and assuming a fully sequential process (third column). The fourth column gives the adopted reaction rate given in the NACRE compilation [16].

of Eq.(10), which implies use of the cross section (6) and consequently inclusion of the energy tail (21) coming from the decay of the 0^+ resonance in ${}^8\text{Be}$. When this is done we obtain the rate given by the thin solid line in Fig. 9, which, as expected, are slightly below the results given in [16] (open circles) at very low temperatures.

Finally, let us assume that the low energy tail in σ_γ corresponds to a direct decay mechanism (dashed curve in the inset of Fig. 8). In this case, the cross section is given by (4), and the low energy tail takes again the form (24). The reaction rate is then given by Eq.(3), and we obtain the thick solid curve in Fig. 9. The reaction rate computed assuming a direct capture at very low energies and the one obtained assuming a sequential capture begin to differ for temperatures smaller than about 0.07 GK. Very soon the rate obtained in the direct picture is several orders of magnitude bigger than the sequential one. This is better appreciated in the inset of the figure, where we show the ratio between both reaction rates. For a temperature of 0.01 GK the reaction rate in the direct picture is almost 7 orders of magnitude bigger than in the sequential picture. The general behavior of the reaction rates is similar to the one obtained for the triple alpha reaction, although due to the smaller Coulomb repulsion, the absolute values of the rates are now much bigger.

As for ${}^{12}\text{C}$, we now give in table 2 the computed reactions rates in the direct picture (second column) and in the sequential picture (third column) for temperatures from 10^{-3} GK to 0.1 GK. In the fourth column we give the adopted value quoted in [16]. As already mentioned, for very low temperatures, our computed rates in the sequential picture are below (up to more than a factor of

4 for $T = 0.001$ GK) the rates given in [16]. In fact, our values are even below the lower limit for the rate given in [16]. When a constant value is taken for the different Γ 's involved in the decay of the $5/2^+$ resonance, a rate within the limits given in [16] is obtained.

The comments made when discussing the reaction rates for the triple alpha reaction are still valid here. First, the computed rates are the limiting cases of a fully direct process and a fully sequential process in the very low energy region. If both processes compete, the computed reaction rate would be found in between the thin and thick solid curves in Fig. 9. And second, the calculation in the direct picture has been made assuming that $\Gamma_\gamma(E)$, given by Eq.(17), is the same as in the sequential picture, with $\Gamma_\gamma = 0.51$ eV. A change in Γ_γ would imply the same change in the reaction rate.

6 Summary and conclusions

In this work we investigate how different descriptions of the photodissociation cross sections at very low energies change the reaction rates for radiative three-body capture processes. We focus on the reaction rates at the very low temperatures relevant for the nucleosynthesis of elements in the core of a star. More precisely, we consider the radiative capture of three particles (nuclei, neutrons, protons...) into a bound nucleus plus a photon. We investigate how the reaction rate for such a process changes at low temperatures depending on the capture mechanism, i.e. either sequentially through an intermediate two-body state or directly.

We first establish notation and definitions, and in particular we specify the formulae for sequential and direct reaction rates for three arbitrary particles. These expressions rely heavily on the energy dependence of the photodissociation cross section. We have previously computed rates and cross sections in a full three-body computation without assumptions of reaction mechanism. In these computations the shape of the cross sections around resonance positions are computed as well, except at very low energies where the discretization is insufficient to characterize the resonance shapes, and a specific form has to be chosen. These low energies are crucial in the present work where we assume a simple Breit-Wigner form for the photodissociation cross section but with energy dependent width as in R -matrix analyses. This is not a severe limitation since the overall conclusions are general and very robust.

We compute rates as functions of the involved parameters for both two- and three-body resonances. We study the dependence on reaction mechanisms for different resonance positions and widths for different combinations of charges. The different rates almost coincide for temperatures somewhat larger than the three-body resonance energy. The direct decay only depends on position and width of the three-body resonance entering through the photodissociation cross section, and thus not on any two-body substructure. On the other hand, the sequential decay mechanism strongly depends on the relative position of the intermediate two-body resonance. If the two-

body resonance is above the three-body resonance and the widths are substantially smaller than the energy difference between these resonances the sequential rate reproduces almost the extreme limit of zero widths where the rate expressions are very simple.

When the two and three-body energies exchange positions much larger rates are found and the sequential and direct rates apparently becomes more similar. However, they still deviate by many orders of magnitude strongly depending on charge and, without Coulomb potentials, angular momentum. In all cases the sequential rate is substantially smaller than the direct rate, except when the two and three-body energies are fairly close to each other and all particles are charged.

We turn to practical and realistic estimates of astrophysical reaction rates. We compute rates for the $\alpha + \alpha + \alpha \rightarrow {}^{12}\text{C} + \gamma$ and the $\alpha + \alpha + n \rightarrow {}^9\text{Be} + \gamma$ reactions. Three-body calculations [12] show that at high temperatures the usual sequential description [15, 16, 29] is appropriate. We focus on the reaction rates at low temperatures, where due to the extremely small energies, clearly below the energy of the available intermediate two-body state, the sequential picture is questionable. Therefore, for high temperatures we take one of the sequential parametrizations of the photodissociation cross section available in the literature. For the low energy tail we consider the possibility of a direct process for which the penetration factors are known for both Coulomb and centrifugal barrier potentials.

We find that a direct description of the low energy tail of the photodissociation cross section enhances the reaction rates at low temperatures by several orders of magnitude compared to the sequential description. For a temperature of 0.01 GK the difference is of about 7 orders of magnitude for the two reactions investigated. These reaction rates in the direct and sequential pictures are the upper and lower limits of the rates. Therefore the result obtained for the triple alpha reaction in [34] is not consistent with our calculation.

In conclusion, comparison between sequential and direct capture mechanisms reveal large differences at temperatures below the three-body resonance energy. These temperatures are important for the capture processes producing light nuclei in aging stars. The traditional use of the sequential models is insufficient and the direct reaction mechanism should be employed for these temperatures. Usually this leads to a substantial enhancement of the rates, but the precise increase depends on the characteristics of the most important resonances. Thus, individual calculations are necessary for each process.

This work was partly supported by funds provided by DGI of MEC (Spain) under contract No. FIS2008-01301. One of us (R.D.) acknowledges support by a Ph.D. I3P grant from CSIC and the European Social Fund.

References

1. M.V. Zhukov, B.V. Danilin, D.V. Fedorov, J.M. Bang, I.J. Thompson, J.S. Vaagen, Phys. Rep. **231**, 151 (1993).

2. E. Nielsen, D.V. Fedorov, A.S. Jensen, E. Garrido, Phys. Rep. **347**, 373 (2001).
3. A. Csótó, Phys. Rev. C **49**, 2244 (1994).
4. S. Aoyama, T. Myo, K. Kato, K. Ikeda, Prog. Theor. Phys. **116**, 1 (2006).
5. R. Alvarez-Rodríguez, E. Garrido, A.S. Jensen, D.V. Fedorov, H.O.U. Fynbo, Eur. Phys. J. A **31**, 303 (2007).
6. E. Garrido, D.V. Fedorov, A.S. Jensen, Phys. Lett. B **684**, 132 (2010).
7. R. Álvarez-Rodríguez, A.S. Jensen, E. Garrido, D.V. Fedorov, Phys. Rev. C **82**, 034001 (2010).
8. R. de Diego, E. Garrido, D.V. Fedorov, A.S. Jensen, Nucl. Phys. A **786**, 71 (2007).
9. T. Myo, K. Kato, S. Aoyama, K. Ikeda, Phys. Rev. C **63**, 054313 (2001).
10. P. Descouvemont, E.M. Tursunov, D. Baye, Nucl. Phys. A **765**, 370 (2006).
11. B.V. Danilin, J.S. Vaagen, T. Rogde, S.N. Ershov, I.J. Thompson, M.V. Zhukov, Phys. Rev. C **76**, 064612 (2007).
12. R. de Diego, E. Garrido, D.V. Fedorov, A.S. Jensen, Europhys. Lett. **90**, 52001 (2010).
13. R. Álvarez-Rodríguez, A.S. Jensen, E. Garrido, D.V. Fedorov, H.O.U. Fynbo, Phys. Rev. C **77**, 064305 (2008).
14. H.O.U. Fynbo, R. Álvarez-Rodríguez, A.S. Jensen, O.S. Kirsebom, D.V. Fedorov, E. Garrido, Phys. Rev. C **79**, 054009 (2009).
15. W. A. Fowler, G. R. Caughlan, B. A. Zimmerman, Annu. Rev. Astron. Astrophys. **5**, 525 (1967).
16. C. Angulo et al., Nucl. Phys. A **656**, 3 (1999).
17. A. Aprahamian, K. Langanke, M. Wiescher, Prog. Part. Nucl. Phys. **54**, 535 (2005).
18. A.M. Mukhamedzhanov et al., J. Phys. G: Nucl. Part. Phys. **31**, S1413 (2005).
19. L.V. Grigorenko, K. Langanke, N.B. Shulgina, M.V. Zhukov, Phys. Lett. B **641**, 254 (2006).
20. R. de Diego, E. Garrido, D.V. Fedorov, A.S. Jensen, Phys. Lett. B **695**, 324 (2011).
21. V.D. Efros, W. Balogh, H. Herndl, R. Hofinger, H. Oberhummer, Z. Phys. A **355**, 101 (1996).
22. H. Oberhummer, A. Csótó, H. Schlattl, Nucl. Phys. A **689**, 269 (2001).
23. D.V. Fedorov, R. de Diego, E. Garrido, A.S. Jensen, J. Phys. G: Nucl. Part. Phys. **37**, 115105 (2010).
24. J. Giovinazzo et al., Phys. Rev. Lett. **89**, 102501 (2002).
25. E. Garrido, D.V. Fedorov, A.S. Jensen, Nucl. Phys. A **733**, 85 (2004).
26. B.S. Meyer, Annu. Rev. Astron. Astrophys. **32**, 153 (1994).
27. A. Bartlett, J. Görres, G.J. Mathews, K. Otsuki, M. Wiescher, D. Frekers, A. Mengoni, and J. Tostevin, Phys. Rev. C **74**, 015802 (2006).
28. R. de Diego, E. Garrido, A.S. Jensen, D.V. Fedorov, Phys. Rev. C **77**, 024001 (2008).
29. K. Sumiyoshi, H. Utsunomiya, S. Goko, T. Kajino, Nucl. Phys. A **709** (2002) 467.
30. R. Álvarez-Rodríguez, H.O.U. Fynbo, A.S. Jensen, E. Garrido, Phys. Rev. Lett. **100**, 192501 (2008).
31. R. Alvarez-Rodríguez, A.S. Jensen, D.V. Fedorov, H.O.U. Fynbo, E. Garrido, Phys. Rev. Lett. **99**, 072503 (2007).
32. M.A. Preston and R.K. Bhaduri, *Structure of the Nucleus*, Addison-Wesley Publishing Company (1975), pp. 672.
33. E. Garrido, D.V. Fedorov, A.S. Jensen, and H.O.U. Fynbo, Nucl. Phys. A **748**, 27 (2005).
34. K. Ogata, M. Kan, M. Kamimura, Prog. Theor. Phys. **122**, 1055 (2009).
35. A. Dotter and B. Paxton, Astron. & Astrophys. **507**, 1617 (2009).
36. R. Álvarez-Rodríguez, A.S. Jensen, E. Garrido, D.V. Fedorov, H.O.U. Fynbo, Phys. Rev. C **77**, 064305 (2008).
37. F. Ajzenberg-Selove, Nucl. Phys. A **490**, 1 (1988).
38. E. Garrido, D.V. Fedorov, A.S. Jensen, Phys. Lett. B **684**, 132 (2010).
39. O. Burda, P. von Neumann-Cosel, A. Richter, C. Forssén, B.A. Brown, Phys. Rev. C **82**, 015808 (2010).